Quantum criticality using a superconducting quantum processor

Maxime Dupont and Joel E. Moore

Phys. Rev. B **106**, L041109 — Published 13 July 2022

DOI: 10.1103/PhysRevB.106.L041109

Quantum Criticality Using a Superconducting Quantum Processor

Maxime Dupont and Joel E. Moore
Department of Physics, University of California, Berkeley, California 94720, USA and
Materials Sciences Division, Lawrence Berkeley National Laboratory, Berkeley, California 94720, USA

Quantum criticality emerges from the collective behavior of many interacting quantum particles, often at the transition between different phases of matter. It is one of the cornerstones of condensed matter physics, which we access on noisy intermediate-scale (NISQ) quantum devices by leveraging a dynamically-driven phenomenon. We probe the critical properties of the one-dimensional quantum Ising model on a programmable superconducting quantum chip via a Kibble–Zurek process, obtain scaling laws, and estimate critical exponents despite inherent sources of errors on the hardware. In addition, we investigate how the improvement of NISQ computers (more qubits, less noise) will consolidate the computation of those universal physical properties. A one-parameter noise model captures the effect of imperfections and reproduces the experimental data. Its systematic study reveals that the noise, analogously to temperature, induces a new length scale in the system. We introduce and successfully verify modified scaling laws, directly accounting for the noise without any prior knowledge. It makes data analyses for extracting physical properties transparent to noise. By understanding how imperfect quantum hardware modifies the genuine properties of quantum states of matter, we enhance the power of NISQ processors considerably for addressing quantum criticality and potentially other phenomena and algorithms.

The advent of quantum computing promises to disrupt nearly every industry, from materials science, chemistry, and drug discovery to security, optimization, as well as artificial intelligence. However, current quantum processors have limited computing capabilities, with only a small number of imperfect qubits available. Although quantum advantage [1] has been claimed on such NISQ devices [2, 3], it is only on specific tasks of narrow interest. Therefore, a major goal is to address practical problems with NISQ machines [4]. Quantum many-body problems, which seek to describe interacting quantum degrees of freedom, provide an ideal playground. Not only are they suitable for current and future NISQ hardware, but they are also of prime importance in basic research. They span nuclear, high-energy, condensed matter, atomic, molecular, optical physics, and quantum chemistry. Only a corner of quantum many-body problems can be solved efficiently with classical computers—these can serve for benchmarking—whereas the vast majority is still open.

For instance, competing interactions between quantum particles can lead to the emergence of exotic phases of matter and phase transitions between them [5, 6]. Of particular interest are quantum many-body systems experiencing a second-order quantum phase transition, as they exhibit quantum criticality [7–9]: an emerging scale-invariance dictating how physical quantities (e.g., susceptibility, specific heat, spectral gap, correlations, etc.) behave close to the transition. Quantum criticality is tabulated into universality classes, defined by a set of critical exponents characterizing the nature of the transition. Remarkably, universality classes are independent of most of the microscopic details of a quantum system and depend instead on general attributes such as dimension and symmetries. Hence, accessing, classifying, and understanding quantum criticality is a formidable fundamental physics challenge. A conventional way for investigating quantum criticality in a quantum many-body system consists of studying its ground state properties as a function of a parameter g driving the transition, with the transition taking place at $g = g_c$, known as the quantum critical point (QCP) [6]. However, obtaining the lowest-energy state of a given Hamiltonian $\hat{\mathcal{H}}(g)$ is a cumbersome task for NISQ devices.

We bypass this obstacle by leveraging a dynamically-driven phenomenon to access quantum criticality, the Kibble–Zurek (KZ) mechanism [10, 11]. NISQ processors have proven to be well-suited in simulating quantum dynamics [12–33], as the time-evolution is a unitary operation that can be straightforwardly translated into a shallow quantum circuit in most cases. The KZ mechanism is triggered by time-evolving a system from a point A to a point B of its phase diagram at a given rate $\sim T^{-1}$, with the transition happening somewhere on the way. With the spectral gap of a quantum system vanishing as $\Delta \sim |g - g_c|^{z\nu}$ close to a second-order phase transition (with $z,\ \nu > 0$ the dynamical and correlation length critical exponents, respectively) [5, 6], we expect a characteristic timescale τ and associated gap scale $\hbar/\tau$, where the adiabaticity of the evolution breaks down. It happens at a dimensionless distance $|g - g_c|/g_c \sim \tau/T$ of the critical point, and one finds that $\tau \sim T^{z\nu/(1+z\nu)}$. Likewise, a characteristic length scale $\ell \sim \tau^{1/z}$ emerges. It diverges in the adiabatic limit, leading to scale invariance, as one would expect in the ground state of $\hat{\mathcal{H}}(g = g_c)$.

Because the KZ mechanism is controlled by the same critical exponents as the static physics, one can exploit it to access key properties of quantum criticality in many-body systems. For example, the KZ process was recently used in a Rydberg atomic simulator to study a quantum critical point [34]. Here, we analyze a classic example of quantum criticality in one spatial dimension through both a gate-based quantum processor and a classical matrix product state computation incorporating noise. We find that the effect of noise is analogous to that of temperature: It induces a length scale that can be accounted for through modified scaling laws. Our results enhance the power of NISQ processors significantly by making data anal-

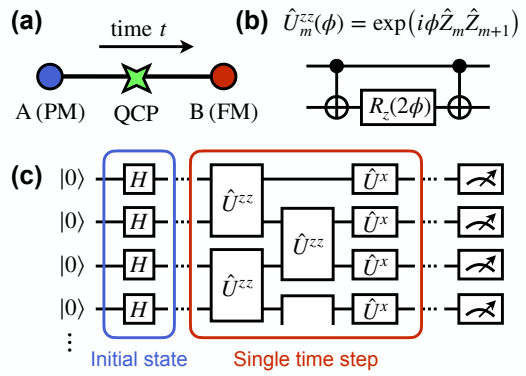

FIG. 1. (a) Quantum system dynamically driven from a point A (paramagnetic phase—PM, for the quantum Ising model considered here) to a point B (ferromagnetic phase—FM) of its phase diagram, with a transition happening on the way, characterized by a quantum critical point (QCP). (b) Decomposition of the operator $\hat{U}^{zz}_m(\phi) = \exp(i\phi\hat{Z}_m\hat{Z}_{m+1})$ by sandwiching a single-qubit rotation gate around the z axis by two-qubit CNOT gates. (c) Quantum circuit for the discretized unitary operation of Eq. (2) for the quantum Ising model (3). The PM ground state is constructed by applying Hadamard gates H on individual qubits. The second step is the time-evolution, generated by a first-order Suzuki-Trotter expansion. Here, $\hat{U}^{x}_m(\phi) = \exp(i\phi\hat{X}_m)$.

yses transparent to inherent noise. Understanding how imperfect quantum hardware modifies the genuine properties of quantum states of matter is a prerequisite for condensed matter simulations, which are doomed to be noisy in the near future.

One may write a Hamiltonian interpolating between points A and B in a KZ process as,

$$\hat{\mathcal{H}}(T,t) = (1 - t/T)\hat{\mathcal{H}}_{\rm A} + (1 + t/T)\hat{\mathcal{H}}_{\rm B}, \tag{1}$$

running from time $t = -T$ to $t = +T$ with $\hat{\mathcal{H}}_{\rm A,B}$ describing A and B, respectively. After initially preparing the system $|\Psi(t = -T)\rangle$ into the ground state of $\hat{\mathcal{H}}_{\rm A}$, it is dynamically driven to point B,

$$\big|\Psi(t)\big\rangle = \mathcal{T}\exp\left[-\frac{i}{\hbar}\int_{-T}^{t} {\rm d}t'\,\hat{\mathcal{H}}(T,t')\right]\big|\Psi(-T)\big\rangle, \tag{2}$$

as pictured in Fig. 1(a). $\mathcal{T}$ indicates a time-ordered exponential. Close to the transition, i.e., around a model-dependent value of t, the KZ mechanism will kick in, and $|\Psi(t)\rangle$ will display universal quantum critical properties. They can be extracted and studied by computing standard observables supplemented with a scaling analysis [35].

We consider the quantum Ising model in one dimension, whose microscopic Hamiltonian interpolates between paramagnetic (PM) ≡A and ferromagnetic (FM) ≡B phases,

$$\hat{\mathcal{H}}_{\rm PM} = -\sum\nolimits_n \hat{X}_n, \quad \text{and} \quad \hat{\mathcal{H}}_{\rm FM} = -\sum\nolimits_n \hat{Z}_n\hat{Z}_{n+1}, \tag{3}$$

with $\hat{X}_n$ and $\hat{Z}_n$ as Pauli operators acting on qubit n. This model presents several advantages: first, it provides the standard paradigm of a solvable QCP at the transition between the two phases. Second, its dynamics can be encoded as a quantum circuit with a relatively low gate count. Third, in the basis where $\hat{Z}$ is diagonal, the starting point (ground state of $\hat{\mathcal{H}}_{\rm PM}$) is an equal superposition of all basis states, which can be readily obtained by applying individual Hadamard gates on each of the qubits. With the interpolation of Eq. (1), it is known that the QCP is located at $t = 0$. Furthermore, the KZ mechanism on the quantum Ising model is extensively documented [34, 36–48].

The evolution operator in Eq. (2) is discretized by making the Hamiltonian operator piecewise constant over a time step δt. Thanks to the locality of the Ising terms in Eq. (3), the exponentiation can be performed using a Suzuki-Trotter expansion [49], at the expense of a systematic—yet controlled—error. It engenders operators of the form $\hat{U}^{x}_m(\phi) = \exp(i\phi\hat{X}_m)$ and $\hat{U}^{zz}_m(\phi) = \exp(i\phi\hat{Z}_m\hat{Z}_{m+1})$, which can be easily translated into standard quantum logic gates. The former is directly related to a single-qubit rotation gate around the x axis, $R_x(\phi)$, and the latter can be decomposed into standard gates [50], see Fig. 1(b). The quantum circuit for one time step using a first-order Suzuki-Trotter expansion is shown in Fig. 1(c).

To investigate quantum criticality, we look at the two-point correlation function,

$$C(T,t,x) = \big\langle\Psi(t)\big|\hat{Z}_r\hat{Z}_{r\pm x}\big|\Psi(t)\big\rangle, \tag{4}$$

between a reference qubit r assumed in the middle of the system and another qubit at distance x. Close to the QCP, it is expected to show a universal behavior of the form [42, 44, 45],

$$C(T,t,x) = \ell^{-\eta}\,\mathcal{F}\big(x/\ell, t/\tau\big), \tag{5}$$

with $\mathcal{F}$ a non-universal scaling function, η the anomalous critical exponent, ℓ and τ the characteristic length and time scales of the KZ mechanism, which depend on T and the critical exponents. ℓ can be interpreted as the length over which the system will be defect-free. From there, one can deduce that the adiabatic limit for a system of size L will be recovered for drive times $T \gtrsim L^{(1+z\nu)/\nu}$—though the point of the KZ mechanism is that useful physics can still be extracted outside of the adiabatic regime.

To verify the scaling law of Eq. (5) we emulate the quantum circuit corresponding to an open chain of $L = 257$ qubits together with a second-order Suzuki-Trotter expansion and time step $\delta t = 0.1$ for different values $T = 8, 16, \ldots 256$. We set $\hbar = 1$. Although it is way out of reach for NISQ hardware, it allows us to obtain benchmark data. The emulation is performed using matrix product states, a well-established and efficient tensor network technique for classically simulating one-dimensional quantum systems [52]. The correlation $C(T, t = 0, x)$ is plotted in Fig. 2(a). We proceed to the rescaling of the data using the exactly known value of the critical exponents of the Ising universality class in 1 + 1 dimensions: $\nu = z = 1$ and $\eta = 1/4$ [53]. The result is displayed in Fig. 2(b) where an excellent data collapse is found. An important point that we make in the Supplemental Material [51] is that, by reducing the standards of an ideal simulation: smaller number

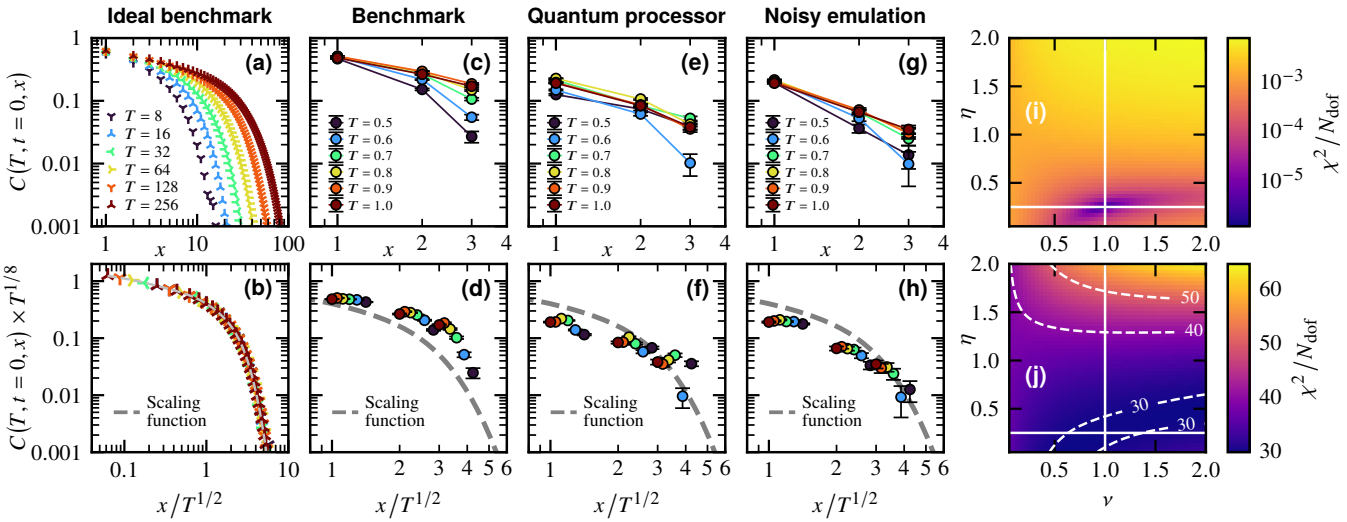

FIG. 2. (a)–(c)–(e)–(g) Two-point correlation function of Eq. (4) at $t = 0$ plotted versus the distance x for different drive times T. (b)–(d)–(f)–(h) Rescaled two-point correlation function according to Eq. (5) with $\nu = z = 1$ and $\eta = 1/4$. (a)–(b) Tensor network emulation of the quantum circuit for $L = 257$ qubits with a second-order Suzuki-Trotter expansion and time step $\delta t = 0.1$. (c)–(d) Perfect emulation of the quantum circuit using $L = 7$ qubits and performing two time steps of different duration δt to access various drive times T. (e)–(f) Simulation on Rigetti Aspen-9 superconducting quantum chip using the same parameters as (a) and (b). (g)–(h) Noisy emulation of the quantum circuit to model the imperfect hardware. (i)–(j) Chi-square per degree of freedom $\chi^2/N_{\rm dof}$ quantifying the quality of the data collapse for the two-point correlation function of Eq. (4) as a function of the critical exponents ν and η, see Supplemental Material [51] (smaller is better). The best collapse should be obtained from the genuine values of ν and η. The exact values are marked at the intersection of the two bold straight white lines. (i) Using the benchmark data of (a). (j) Using the quantum processor data of (e).

of qubits, larger time step, lower-order Suzuki-Trotter expansion, and shorter drive times T, one is still able to produce reasonable physics that should be accessible on current NISQ devices, see also Figs. 2(c)–(d).

We now run the quantum circuit on a quantum computer. We use Rigetti Aspen-9 superconducting quantum chip and the provided compiler to translate the quantum circuit into the native gate set [51]. We work with seven qubits, each directly representing one Ising spin of the Hamiltonians (3). We perform two time steps using a first-order Suzuki-Trotter expansion, and vary its duration δt to access different drive times T. We collect 32 768 basis states as outputs, from which we compute the two-point correlation function of Eq. (4). The raw data are shown in Fig. 2(d). We observe a distinct decay of the correlation with the distance, but there is no clear hierarchy for the different T values, although the smaller ones tend to be generally lower. Note that, unlike the benchmark emulation, the range of available drive times and distances is more restricted. In the corresponding lower panel, we rescale the data according to Eq. (5) and plot for comparison the scaling function extracted from the benchmark data of Fig. 2(b). There is a good qualitative agreement, despite the hardware being imperfect.

By leaving the exponents ν and η as free parameters and solving the optimization problem seeking to maximize the quality of the data collapse (e.g., by minimizing the chi-square per degree of freedom $\chi^2/N_{\rm dof}$) [51, 54], we can extract a region of maximum likelihood for their values. The corresponding results for the benchmark and quantum processor data are shown in Figs. 2(i)–(j). The procedure on the benchmark data gives back the known values of the critical exponents. As for the experimental data, we are not able to precisely determine values for the exponents, as there is no clear minimum for the chi-square (cause by a smaller number of qubits, a smaller range of drive times T, noise, etc.). Nonetheless, we find that the exact values are within the region with minimum $\chi^2/N_{\rm dof}$, and which provides bounds for the exponents. We expect that the continuous improvement of NISQ processors will tighten the bound on the exponent values, see Supplemental Material for additional data [51].

Noise is inherent in NISQ devices, has various origins, and is by definition machine-specific. Familiar sources include decoherence through relaxation and dephasing, readout error, and the qubits being imperfect two-level systems, which can result in faulty quantum operations. Here, we model the effect of noise with a depolarizing channel [55]. The noisy system is emulated by performing the following stochastic modification to the quantum logic gates [56, 57],

$$\begin{cases} \hat{G}_m & \to \hat{G}_m \hat{\mathfrak{a}}_m, \\ \hat{G}_{m,n} & \to \hat{G}_{m,n}(\hat{\mathfrak{a}}_m \otimes \hat{\mathfrak{b}}_n), \end{cases} \quad \hat{\mathfrak{a}}, \hat{\mathfrak{b}} \in \{\hat{I}, \hat{X}, \hat{Y}, \hat{Z}\}, \tag{6}$$

where $\hat{G}_m$ and $\hat{G}_{m,n}$ represent a one-qubit acting on m and a two-qubit gate acting on (m, n), respectively. The probability that it remains unchanged, i.e., $\hat{\mathfrak{a}}(= \hat{\mathfrak{b}}) = \hat{I}$, is $1 - p$, with p a parameter controlling the strength of noise. All other

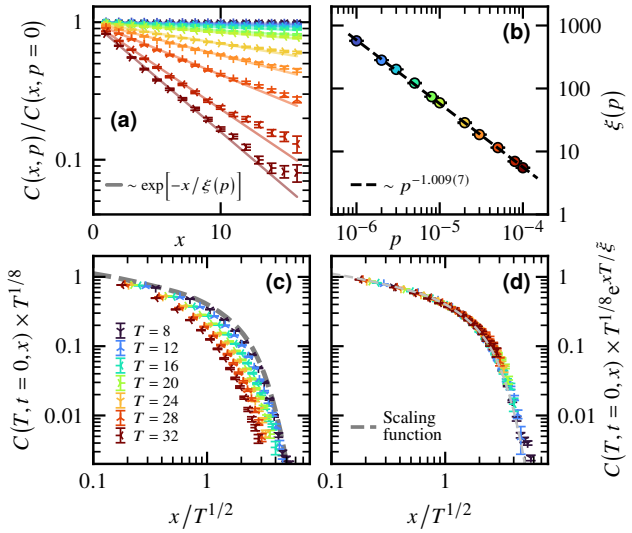

FIG. 3. (a) Two-point correlation of Eq. (4) as a function of the distance x, rescaled by the $p = 0$ data for $L = 33$ qubits. Emulation details: 36 513 gates comprised of Hadamard, $\hat{U}^x$, and $\hat{U}^{zz}$ with $T = 32$, $t = 0$, and second-order Suzuki-Trotter expansion where $\delta t = 0.1$. The results are averaged over $\gtrsim 2 \times 10^3$ random circuits. Each curve corresponds to a value of p whose code color can be read from panel (b). Fit of the observed exponential decay $\sim \exp\left[-x/\xi(p)\right]$ (bold line) to extract length $\xi(p)$. (b) Length $\xi(p)$ as a function of p, which shows a $\sim 1/p$ dependence. (c)–(d) Rescaled two-point correlation function according to Eq. (5) ($z = \nu = 1$ and $\eta = 1/4$). The form of the circuit is the same as the one in panel (a) with $p = 10^{-4}$ for various drive times T. (d) Same as (c) except that the y-axis is multiplied by an additional term with $\tilde{\xi} \approx 180$, see Eq. (7).

combinations are uniformly distributed with probabilities $p/3$ and $p/15$ for one- and two-qubit gates, respectively. The process has to be repeated many times to generate random disordered circuits over which the results are averaged. The $\hat{Z}$ gates induce dephasing, the $\hat{X}$ gates induce a qubit flip, and $\hat{Y}$ a mix of the two.

To assess the reasonableness of the noise model of Eq. (6), we emulate the experiment in the presence of noise and attempt to find a value for the parameter p, reproducing at best the experimental data of Figs. 2(e)–(f). Because all the circuits run on the quantum processor involve two time steps using a first-order Suzuki-Trotter expansion, they all have the same form and size: we anticipate that different quantum circuits performing the same task (following, e.g., compilation) will simply lead to a rescaled value of the phenomenological parameter p. To that end, we emulate with noise the circuit of Fig. 1(c). We report the results in Figs. 2(g)–(h) for $p \approx 0.08$. Despite being a simple one-parameter phenomenological model which may not capture the various imperfections of the hardware, a good agreement with the experimental data is observed, thus validating to some extent the model.

To better understand the physics induced by the noise model on the time-evolution, we study the combined systems as a function of p using matrix product states. The form and size of the circuit are fixed with $L = 33$ qubits and 36 513 gates. We plot in Fig. 3(a) the two-point correlation function of Eq. (4) rescaled by the noiseless data as a function of the distance x. We observe an exponential decay of the form $C(x,p) = C(x,p=0)e^{-x/\xi(p)}$, meaning that the noise gives rise to a new length scale in the system. We extract it in Fig. 3(b) and find that $\xi(p) \sim 1/p$. A simple argument where one supposes that the effect of a single defect in a circuit volume dx (with d the depth) will reduce the correlation by a factor $\varepsilon > 1$, leads to $C(x,p) \sim C(x,p=0)/\varepsilon^{pdx}$ for an average number of defects $\sim pdx$, assuming their effect is uncorrelated. It is compatible with the exponential decay observed in the emulations reported in Figs. 3(a)–(b). The depth-dependence $\xi \sim 1/d$ at fixed p is verified in the Supplemental Material [51]. Note that for a fixed time step δt, the circuit depth is proportional to the drive time T, and we use $d \to T$ in the following. The noise-induced length scale $\xi \sim 1/pT$ competes with the characteristic length scale $\ell \sim T^{\nu/(1+z\nu)}$ of the KZ mechanism. In the one-dimensional quantum Ising model studied here, for the KZ mechanism to dominate over the noise and observe genuine quantum criticality, one needs $p \ll T^{-3/2} \sim L^{-3}$. An analogy can be drawn between the noise in the quantum circuit and thermal effects induced by a finite temperature Θ in the quantum Ising model, as they both lead to a length scale $\xi^{-1} \sim \Theta \sim p$ [58]. Such an analogy between noise and effective temperature was also reported in open quantum systems [59–61] and sudden quench protocols subject to a time-dependent white noise [62, 63]. Interestingly, one can include a new parameter $\tilde{\xi} = T\xi$ in the critical scaling of Eq. (5), accounting for the effect of noise on quantum criticality,

$$\mathcal{F}\left(x/\ell, t/\tau\right) \;\to\; \mathcal{F}\left(x/\ell, t/\tau\right) \times \exp\left(-xT/\tilde{\xi}\right). \qquad (7)$$

Eq. (7) is confirmed by emulations based on matrix product state for $L = 33$ qubits and $p = 10^{-4}$, with the form of the circuit and other parameters similar to those of Figs. 3(a)–(b). The raw and noise-corrected data collapses are displayed side by side in Figs. 3(c)–(d), with a substantial improvement upon including the parameter $\tilde{\xi} \approx 180$, which can be found without any prior knowledge, comparably to the critical exponents [51]. The reduced connectivity at the boundaries of the system makes the exponential decay of Fig. 3(a) drifts for these qubits, and the noise correction is not directly applicable on smaller-scale systems, such as the ones simulated on the quantum processor displayed in Figs. 2(e)–(f).

While quantum criticality is well-understood in $1+1$ dimensions, much less is known beyond that. The absence of efficient classical methods to simulate certain types of quantum many-body systems, e.g., interacting fermions or frustrated magnets, limits our microscopic understanding of these phases of matter and their transitions. Here, we have shown that current NISQ devices can simulate quantum criticality by leveraging a dynamically-driven phenomenon. Using a programmable superconducting processor, we demonstrated this approach on the one-dimensional quantum Ising model by obtaining a good agreement with benchmark data. Despite the limited number of qubits and the restricted depth of the quantum circuits, we

estimated the critical exponents. The continuous improvement of NISQ hardware will generate better quality and larger-scale data. Not only will it leads to more accurate results, but it will also open the way to uncharted problems. In addition, we have shown that one can directly account for the inherent noise of the current generation of quantum computers. We found that the noise induces a length scale controlling how far qubits can be nontrivially correlated. It can be included in scaling laws, thus making the noise irrelevant to some extent when investigating quantum criticality. Whether this noise-induced length scale is a general feature arising in other quantum algorithms remains to be explored, as similar behavior was recently reported in other kinds of many-body problems [64, 65].

We gratefully acknowledge the support of B. Evert, M. Hodson, M. Paini, and M.J. Reagor at Rigetti Computing. M.D. also acknowledges discussions with A. Avdoshkin, E.G. Dalla Torre, F. Machado, T. Scaffidi, and N.E. Sherman. We thank one of the anonymous referees for suggesting us to consider the strong noise regime [51]. M.D. received support from the U.S. Department of Energy, Office of Science, Office of Basic Energy Sciences, Materials Sciences and Engineering Division under Award No. DE-AC02-05-CH11231 through the Theory Institute for Materials and Energy Spectroscopy (TIMES). J.E.M. was supported by the Quantum Science Center (QSC), a National Quantum Information Science Research Center of the U.S. Department of Energy (DOE), and a Simons Investigatorship. This research used the Lawrencium computational cluster resource provided by the IT Division at the Lawrence Berkeley National Laboratory (supported by the Director, Office of Science, Office of Basic Energy Sciences, of the U.S. Department of Energy under Award No. DE-AC02-05CH11231). This research also used resources of the National Energy Research Scientific Computing Center (NERSC), a U.S. Department of Energy Office of Science User Facility operated under Award No. DE-AC02-05CH11231. In addition, this research used resources of the Oak Ridge Leadership Computing Facility at the Oak Ridge National Laboratory, which is supported by the Office of Science of the U.S. Department of Energy under Award No. DE-AC05-00OR22725.

[1] A. W. Harrow and A. Montanaro, Quantum computational supremacy, Nature **549**, 203 (2017).

[2] F. Arute, K. Arya, R. Babbush, D. Bacon, J. C. Bardin, R. Barends, R. Biswas, S. Boixo, F. G. S. L. Brandao, D. A. Buell, B. Burkett, Y. Chen, Z. Chen, B. Chiaro, R. Collins, W. Courtney, A. Dunsworth, E. Farhi, B. Foxen, A. Fowler, C. Gidney, M. Giustina, R. Graff, K. Guerin, S. Habegger, M. P. Harrigan, M. J. Hartmann, A. Ho, M. Hoffmann, T. Huang, T. S. Humble, S. V. Isakov, E. Jeffrey, Z. Jiang, D. Kafri, K. Kechedzhi, J. Kelly, P. V. Klimov, S. Knysh, A. Korotkov, F. Kostritsa, D. Landhuis, M. Lindmark, E. Lucero, D. Lyakh, S. Mandrà, J. R. McClean, M. McEwen, A. Megrant, X. Mi, K. Michielsen, M. Mohseni, J. Mutus, O. Naaman, M. Neeley, C. Neill, M. Y. Niu, E. Ostby, A. Petukhov, J. C. Platt, C. Quintana, E. G. Rieffel, P. Roushan, N. C. Rubin, D. Sank, K. J. Satzinger, V. Smelyanskiy, K. J. Sung, M. D. Trevithick, A. Vainsencher, B. Villalonga, T. White, Z. J. Yao, P. Yeh, A. Zalcman, H. Neven, and J. M. Martinis, Quantum supremacy using a programmable superconducting processor, Nature **574**, 505 (2019).

[3] M. Gong, S. Wang, C. Zha, M.-C. Chen, H.-L. Huang, Y. Wu, Q. Zhu, Y. Zhao, S. Li, S. Guo, H. Qian, Y. Ye, F. Chen, C. Ying, J. Yu, D. Fan, D. Wu, H. Su, H. Deng, H. Rong, K. Zhang, S. Cao, J. Lin, Y. Xu, L. Sun, C. Guo, N. Li, F. Liang, V. M. Bastidas, K. Nemoto, W. J. Munro, Y.-H. Huo, C.-Y. Lu, C.-Z. Peng, X. Zhu, and J.-W. Pan, Quantum computational advantage using photons, Science **370**, 1460 (2020).

[4] J. Preskill, Quantum Computing in the NISQ era and beyond, Quantum **2**, 79 (2018).

[5] M. Vojta, Quantum phase transitions, Rep. Prog. Phys. **66**, 2069 (2003).

[6] S. Sachdev, *Quantum Phase Transitions*, 2nd ed. (Cambridge University Press, 2011).

[7] J. A. Hertz, Quantum critical phenomena, Phys. Rev. B **14**, 1165 (1976).

[8] R. B. Laughlin, G. G. Lonzarich, P. Monthoux, and D. Pines, The quantum criticality conundrum, Adv. Phys. **50**, 361 (2001).

[9] P. Coleman and A. J. Schofield, Quantum criticality, Nature **433**, 226 (2005).

[10] T. W. B. Kibble, Topology of cosmic domains and strings, J. Phys. A Math. **9**, 1387 (1976).

[11] W. H. Zurek, Cosmological experiments in superfluid helium?, Nature **317**, 505 (1985).

[12] R. Barends, L. Lamata, J. Kelly, L. García-Álvarez, A. G. Fowler, A. Megrant, E. Jeffrey, T. C. White, D. Sank, J. Y. Mutus, B. Campbell, Y. Chen, Z. Chen, B. Chiaro, A. Dunsworth, I. C. Hoi, C. Neill, P. J. J. O'Malley, C. Quintana, P. Roushan, A. Vainsencher, J. Wenner, E. Solano, and J. M. Martinis, Digital quantum simulation of fermionic models with a superconducting circuit, Nat. Commun. **6**, 7654 (2015).

[13] A. A. Zhukov, S. V. Remizov, W. V. Pogosov, and Y. E. Lozovik, Algorithmic simulation of far-from-equilibrium dynamics using quantum computer, Quantum Inf. Process. **17**, 223 (2018).

[14] N. Klco, E. F. Dumitrescu, A. J. McCaskey, T. D. Morris, R. C. Pooser, M. Sanz, E. Solano, P. Lougovski, and M. J. Savage, Quantum-classical computation of schwinger model dynamics using quantum computers, Phys. Rev. A **98**, 032331 (2018).

[15] H. Lamm and S. Lawrence, Simulation of nonequilibrium dynamics on a quantum computer, Phys. Rev. Lett. **121**, 170501 (2018).

[16] A. Cervera-Lierta, Exact Ising model simulation on a quantum computer, Quantum **2**, 114 (2018).

[17] A. Chiesa, F. Tacchino, M. Grossi, P. Santini, I. Tavernelli, D. Gerace, and S. Carretta, Quantum hardware simulating four-dimensional inelastic neutron scattering, Nat. Phys. **15**, 455 (2019).

[18] A. Smith, M. S. Kim, F. Pollmann, and J. Knolle, Simulating quantum many-body dynamics on a current digital quantum computer, npj Quantum Inf. **5**, 106 (2019).

[19] A. Francis, J. K. Freericks, and A. F. Kemper, Quantum computation of magnon spectra, Phys. Rev. B **101**, 014411 (2020).

[20] S.-H. Lin, R. Dilip, A. G. Green, A. Smith, and F. Pollmann, Real- and imaginary-time evolution with compressed quantum circuits, PRX Quantum **2**, 010342 (2021).

[21] X. Mi, P. Roushan, C. Quintana, S. Mandrà, J. Marshall, C. Neill, F. Arute, K. Arya, J. Atalaya, R. Babbush, J. C. Bardin, R. Barends, J. Basso, A. Bengtsson, S. Boixo, A. Bourassa, M. Broughton, B. B. Buckley, D. A. Buell, B. Burkett, N. Bushnell, Z. Chen, B. Chiaro, R. Collins, W. Courtney, S. Demura,

A. R. Derk, A. Dunsworth, D. Eppens, C. Erickson, E. Farhi, A. G. Fowler, B. Foxen, C. Gidney, M. Giustina, J. A. Gross, M. P. Harrigan, S. D. Harrington, J. Hilton, A. Ho, S. Hong, T. Huang, W. J. Huggins, L. B. Ioffe, S. V. Isakov, E. Jeffrey, Z. Jiang, C. Jones, D. Kafri, J. Kelly, S. Kim, A. Kitaev, P. V. Klimov, A. N. Korotkov, F. Kostritsa, D. Landhuis, P. Laptev, E. Lucero, O. Martin, J. R. McClean, T. McCourt, M. McEwen, A. Megrant, K. C. Miao, M. Mohseni, S. Montazeri, W. Mruczkiewicz, J. Mutus, O. Naaman, M. Neeley, M. Newman, M. Y. Niu, T. E. O'Brien, A. Opremcak, E. Ostby, B. Pato, A. Petukhov, N. Redd, N. C. Rubin, D. Sank, K. J. Satzinger, V. Shvarts, D. Strain, M. Szalay, M. D. Trevithick, B. Villalonga, T. White, Z. J. Yao, P. Yeh, A. Zalcman, H. Neven, I. Aleiner, K. Kechedzhi, V. Smelyanskiy, and Y. Chen, Information scrambling in quantum circuits, Science **0**, eabg5029.

[22] X.-Y. Guo, Z.-Y. Ge, H. Li, Z. Wang, Y.-R. Zhang, P. Song, Z. Xiang, X. Song, Y. Jin, L. Lu, K. Xu, D. Zheng, and H. Fan, Observation of bloch oscillations and wannier-stark localization on a superconducting quantum processor, npj Quantum Inf. **7**, 51 (2021).

[23] B. Fauseweh and J.-X. Zhu, Digital quantum simulation of non-equilibrium quantum many-body systems, Quantum Inf. Process. **20**, 138 (2021).

[24] M. R. Geller, A. Arrasmith, Z. Holmes, B. Yan, P. J. Coles, and A. Sornborger, Quantum simulation of operator spreading in the chaotic ising model, arXiv:2106.16170 (2021).

[25] J. Vovrosh and J. Knolle, Confinement and entanglement dynamics on a digital quantum computer, Sci. Rep. **11**, 11577 (2021).

[26] J. Randall, C. E. Bradley, F. V. van der Gronden, A. Galicia, M. H. Abobeih, M. Markham, D. J. Twitchen, F. Machado, N. Y. Yao, and T. H. Taminiau, Many-body-localized discrete time crystal with a programmable spin-based quantum simulator, Science **0**, eabk0603.

[27] P. T. Dumitrescu, J. Bohnet, J. Gaebler, A. Hankin, D. Hayes, A. Kumar, B. Neyenhuis, R. Vasseur, and A. C. Potter, Realizing a dynamical topological phase in a trapped-ion quantum simulator, arXiv:2107.09676 (2021).

[28] X. Mi, M. Ippoliti, C. Quintana, A. Greene, Z. Chen, J. Gross, F. Arute, K. Arya, J. Atalaya, R. Babbush, J. C. Bardin, J. Basso, A. Bengtsson, A. Bilmes, A. Bourassa, L. Brill, M. Broughton, B. B. Buckley, D. A. Buell, B. Burkett, N. Bushnell, B. Chiaro, R. Collins, W. Courtney, D. Debroy, S. Demura, A. R. Derk, A. Dunsworth, D. Eppens, C. Erickson, E. Farhi, A. G. Fowler, B. Foxen, C. Gidney, M. Giustina, M. P. Harrigan, S. D. Harrington, J. Hilton, A. Ho, S. Hong, T. Huang, A. Huff, W. J. Huggins, L. B. Ioffe, S. V. Isakov, J. Iveland, E. Jeffrey, Z. Jiang, C. Jones, D. Kafri, T. Khattar, S. Kim, A. Kitaev, P. V. Klimov, A. N. Korotkov, F. Kostritsa, D. Landhuis, P. Laptev, J. Lee, K. Lee, A. Locharla, E. Lucero, O. Martin, J. R. McClean, T. McCourt, M. McEwen, K. C. Miao, M. Mohseni, S. Montazeri, W. Mruczkiewicz, O. Naaman, M. Neeley, C. Neill, M. Newman, M. Y. Niu, T. E. O'Brien, A. Opremcak, E. Ostby, B. Pato, A. Petukhov, N. C. Rubin, D. Sank, K. J. Satzinger, V. Shvarts, Y. Su, D. Strain, M. Szalay, M. D. Trevithick, B. Villalonga, T. White, Z. J. Yao, P. Yeh, J. Yoo, A. Zalcman, H. Neven, S. Boixo, V. Smelyanskiy, A. Megrant, J. Kelly, Y. Chen, S. L. Sondhi, R. Moessner, K. Kechedzhi, V. Khemani, and P. Roushan, Time-crystalline eigenstate order on a quantum processor, Nature **601**, 531 (2022).

[29] H. Xu, J. Zhang, J. Han, Z. Li, G. Xue, W. Liu, Y. Jin, and H. Yu, Realizing discrete time crystal in an one-dimensional superconducting qubit chain, arXiv:2108.00942 (2021).

[30] S. K. Zhao, Z.-Y. Ge, Z. Xiang, G. M. Xue, H. S. Yan, Z. T. Wang, Z. Wang, H. K. Xu, F. F. Su, Z. H. Yang, H. Zhang, Y.-R. Zhang, X.-Y. Guo, K. Xu, Y. Tian, H. F. Yu, D. N. Zheng, H. Fan, and S. P. Zhao, Probing operator spreading via Floquet engineering in a superconducting circuit, arXiv:2108.01276 (2021).

[31] L. Bassman, R. V. Beeumen, E. Younis, E. Smith, C. Iancu, and W. A. de Jong, Constant-depth circuits for dynamic simulations of materials on quantum computers, arXiv:2103.07429 (2021).

[32] M. Urbanek, B. Nachman, V. R. Pascuzzi, A. He, C. W. Bauer, and W. A. de Jong, Mitigating depolarizing noise on quantum computers with noise-estimation circuits, arXiv:2103.08591 (2021).

[33] E. Kökcü, D. Camps, L. Bassman, J. K. Freericks, W. A. de Jong, R. V. Beeumen, and A. F. Kemper, Mitigating depolarizing noise on quantum computers with noise-estimation circuits, arXiv:2108.03282 (2021).

[34] S. Ebadi, T. T. Wang, H. Levine, A. Keesling, G. Semeghini, A. Omran, D. Bluvstein, R. Samajdar, H. Pichler, W. W. Ho, S. Choi, S. Sachdev, M. Greiner, V. Vuletić, and M. D. Lukin, Quantum phases of matter on a 256-atom programmable quantum simulator, Nature **595**, 227 (2021).

[35] M. E. Fisher and M. N. Barber, Scaling theory for finite-size effects in the critical region, Phys. Rev. Lett. **28**, 1516 (1972).

[36] W. H. Zurek, U. Dorner, and P. Zoller, Dynamics of a quantum phase transition, Phys. Rev. Lett. **95**, 105701 (2005).

[37] J. Dziarmaga, Dynamics of a quantum phase transition: Exact solution of the quantum Ising model, Phys. Rev. Lett. **95**, 245701 (2005).

[38] L. Cincio, J. Dziarmaga, M. M. Rams, and W. H. Zurek, Entropy of entanglement and correlations induced by a quench: Dynamics of a quantum phase transition in the quantum Ising model, Phys. Rev. A **75**, 052321 (2007).

[39] J. Dziarmaga, Dynamics of a quantum phase transition and relaxation to a steady state, Adv. Phys. **59**, 1063 (2010).

[40] B. Damski, H. T. Quan, and W. H. Zurek, Critical dynamics of decoherence, Phys. Rev. A **83**, 062104 (2011).

[41] R. Puebla, O. Marty, and M. B. Plenio, Quantum Kibble-Zurek physics in long-range transverse-field Ising models, Phys. Rev. A **100**, 032115 (2019).

[42] M. Kolodrubetz, B. K. Clark, and D. A. Huse, Nonequilibrium dynamic critical scaling of the quantum Ising chain, Phys. Rev. Lett. **109**, 015701 (2012).

[43] M. Gong, X. Wen, G. Sun, D.-W. Zhang, D. Lan, Y. Zhou, Y. Fan, Y. Liu, X. Tan, H. Yu, Y. Yu, S.-L. Zhu, S. Han, and P. Wu, Simulating the kibble-zurek mechanism of the ising model with a superconducting qubit system, Sci. Rep. **6**, 22667 (2016).

[44] A. Chandran, A. Erez, S. S. Gubser, and S. L. Sondhi, Kibble-Zurek problem: Universality and the scaling limit, Phys. Rev. B **86**, 064304 (2012).

[45] A. Francuz, J. Dziarmaga, B. Gardas, and W. H. Zurek, Space and time renormalization in phase transition dynamics, Phys. Rev. B **93**, 075134 (2016).

[46] M. M. Rams, J. Dziarmaga, and W. H. Zurek, Symmetry breaking bias and the dynamics of a quantum phase transition, Phys. Rev. Lett. **123**, 130603 (2019).

[47] A. Keesling, A. Omran, H. Levine, H. Bernien, H. Pichler, S. Choi, R. Samajdar, S. Schwartz, P. Silvi, S. Sachdev, P. Zoller, M. Endres, M. Greiner, V. Vuletić, and M. D. Lukin, Quantum Kibble–Zurek mechanism and critical dynamics on a programmable Rydberg simulator, Nature **568**, 207 (2019).

[48] M. Schmitt, M. M. Rams, J. Dziarmaga, M. Heyl, and W. H. Zurek, Quantum phase transition dynamics in the two-dimensional transverse-field Ising model, arXiv:2106.09046 (2021).

[49] N. Hatano and M. Suzuki, Finding exponential product formulas of higher orders, in *Quantum Annealing and Other Optimization Methods*, edited by A. Das and B. K. Chakrabarti (Springer Berlin Heidelberg, Berlin, Heidelberg, 2005) pp. 37–68.

[50] F. Vatan and C. Williams, Optimal quantum circuits for general two-qubit gates, Phys. Rev. A **69**, 032315 (2004).

[51] See Supplemental Material for more information on the quantum circuits implementation, the emulation techniques, additional emulation data studying the effect of the different parameters, details on how the critical exponents are extracted, additional data on the noise model, and details regarding the quantum hardware, which includes Refs. [49, 52, 64, 66–71].

[52] U. Schollwöck, The density-matrix renormalization group in the age of matrix product states, Ann. Phys. **326**, 96 (2011).

[53] P. Francesco, P. Mathieu, and D. Sénéchal, *Conformal Field Theory* (Springer, New York, NY, 1997).

[54] A. W. Sandvik, Computational studies of quantum spin systems, AIP Conf. Proc. **1297**, 135 (2010).

[55] M. A. Nielsen and I. L. Chuang, *Quantum Computation and Quantum Information: 10th Anniversary Edition*, 10th ed. (Cambridge University Press, 2010).

[56] N. Gisin, Quantum measurements and stochastic processes, Phys. Rev. Lett. **52**, 1657 (1984).

[57] J. Dalibard, Y. Castin, and K. Mølmer, Wave-function approach to dissipative processes in quantum optics, Phys. Rev. Lett. **68**, 580 (1992).

[58] S. Sachdev, Finite temperature correlations of the Ising chain in a transverse field, Int. J. Mod. Phys. A **11**, 57 (1997).

[59] M. F. Maghrebi and A. V. Gorshkov, Nonequilibrium many-body steady states via keldysh formalism, Phys. Rev. B **93**, 014307 (2016).

[60] D. A. Paz and M. F. Maghrebi, Driven-dissipative ising model: Dynamical crossover at weak dissipation, arXiv:1906.08278 (2019).

[61] D. A. Paz and M. F. Maghrebi, Driven-dissipative ising model: An exact field-theoretical analysis, Phys. Rev. A **104**, 023713 (2021).

[62] J. Marino and A. Silva, Relaxation, prethermalization, and diffusion in a noisy quantum ising chain, Phys. Rev. B **86**, 060408 (2012).

[63] J. Marino and A. Silva, Nonequilibrium dynamics of a noisy quantum ising chain: Statistics of work and prethermalization after a sudden quench of the transverse field, Phys. Rev. B **89**, 024303 (2014).

[64] M. Ippoliti, K. Kechedzhi, R. Moessner, S. Sondhi, and V. Khemani, Many-body physics in the nisq era: Quantum programming a discrete time crystal, PRX Quantum **2**, 030346 (2021).

[65] J. Richter and A. Pal, Simulating hydrodynamics on noisy intermediate-scale quantum devices with random circuits, Phys. Rev. Lett. **126**, 230501 (2021).

[66] G. Vidal, Efficient simulation of one-dimensional quantum many-body systems, Phys. Rev. Lett. **93**, 040502 (2004).

[67] M. Fishman, S. R. White, and E. M. Stoudenmire, The ITensor software library for tensor network calculations, arXiv:2007.14822 (2020).

[68] C. Developers, Cirq (2021), See full list of authors on Github: https://github .com/quantumlib/Cirq/graphs/contributors.

[69] Q. A. team and collaborators, qsim (2021).

[70] R. S. Smith, E. C. Peterson, M. G. Skilbeck, and E. J. Davis, A Practical Quantum Instruction Set Architecture, arXiv:1608.03355 (2016).

[71] B. C. Dias, M. Haque, P. Ribeiro, and P. McClarty, Diffusive operator spreading for random unitary free fermion circuits, arXiv:2102.09846 (2021).